ACS APPLIED ELECTRONIC MATERIALS

pubs.acs.org/acsaelm Article

Internal Photoemission Spectroscopy Measurements of Interfacial Energy Barriers in Operating TaN/$Hf_{0.5}Zr_{0.5}O_2$/TaN Metal/Ferroelectric/Metal (MFM) Devices

Jessica Haglund, Takanori Mimura, Jon F. Ihlefeld, and John F. Conley, Jr.*

Cite This: *ACS Appl. Electron. Mater.* 2024, 6, 3249−3256 Read Online

ACCESS | Metrics & More | Article Recommendations

ABSTRACT: The effect of the "waking" and subsequent "poling" operations on the electron barriers at both top and bottom electrode interfaces in operating ferroelectric hafnium zirconium oxide ($Hf_{0.5}Zr_{0.5}O_2$, HZO) metal/ferroelectric/metal (MFM) devices are measured for the first time via internal photoemission (IPE) spectroscopy. Top and bottom (TaN/HZO and HZO/TaN) barriers for pristine devices were measured at 2.6 and 2.9 eV, respectively. The waking operation (10 kHz bipolar voltage cycling above the coercive field) increased the top barrier to 2.8 eV while leaving the bottom barrier essentially unchanged. Poling operations (application of a longer 10 ms unipolar pulse) were found to significantly decrease both top and bottom barriers. The poling direction (polarity) had relatively little impact. The barrier for the top interface under positive (P↓) and negative poling (P↑) was 2.1 and 2.2 eV, respectively, while the bottom barrier was 2.3 eV for P↓ and 2.4 eV for P↑. All barrier heights remained unchanged after several months at room temperature. Potential physical mechanisms responsible for the changes observed under electrical operation are consistent with movement and/or creation of charged oxygen vacancy defects.

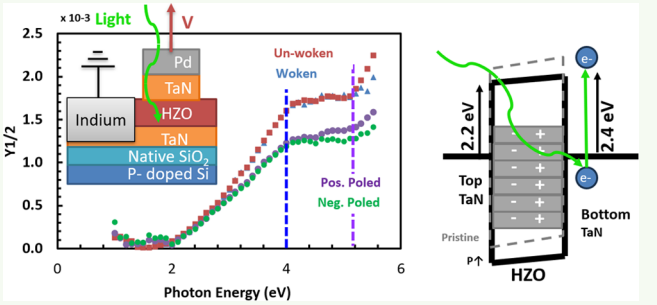

KEYWORDS: *ferroelectricity, HZO, wake-up effect, MIM, ALD*

1. INTRODUCTION

Exponentially increasing energy usage for computation, driven by data centers and artificial intelligence applications, is rapidly approaching worldwide energy production and may soon limit growth of computational capacity.[1,2] Computing technologies with increased energy efficiency are needed. Ferroelectric materials have long attracted interest for applications in ferroelectric random access memory (FeRAM), negative capacitance field effect transistors (NC-FETs), ferroelectric tunnel junctions (FTJs), and high-*k* capacitors.[3−5] These applications are of particular interest for lowering the energy cost associated with computing. Since the first report in 2011 of ferroelectric behavior in thin-film-doped HfO_2,[6] Zr-substituted HfO_2 ($Hf_{1-x}Zr_xO_2$ or HZO) has become a leading candidate ferroelectric material for Si complementary metal oxide semiconductor (CMOS) technology.[7−9] This is primarily due to the potential ease of HZO integration, as HfO_2-based materials are already widely used as the gate dielectrics. To fully understand the operation of electronic devices constructed with HZO, knowledge of the electron energy barriers or band offsets between HZO and adjacent metal electrodes in operating devices is required. In FTJs, for example, the tunneling electroresistance (TER) is thought to depend critically on changes in barrier height.[10] The standard Kraut X-ray photoelectron spectroscopy (XPS) method of determining band offsets requires three different samples and does not represent operational devices.[11] Hard X-ray photoelectron spectroscopy (HX-PES) has been used to measure the top electrode/HZO interface of devices during operation; however, HX-PES requires access to synchrotron facilities, and the >10s of μm diameter probe sizes make measuring individual devices challenging.[12] In contrast, internal photoemission (IPE) spectroscopy allows straightforward "in situ" measurement of both top and bottom internal barriers inside *operating* devices. IPE spectroscopy is an optoelectronic technique that involves measurements of current in a biased device while under simultaneous ultraviolet illumination.[11,13,20] A previous comparison of XPS and IPE measurements on a similar materials system has shown that XPS measurements are insensitive to trapped charge, which is known to play critical

Received: January 11, 2024
Revised: April 5, 2024
Accepted: April 23, 2024
Published: April 30, 2024

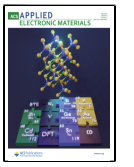

https://doi.org/10.1021/acsaelm.4c00073
ACS Appl. Electron. Mater. 2024, 6, 3249−3256

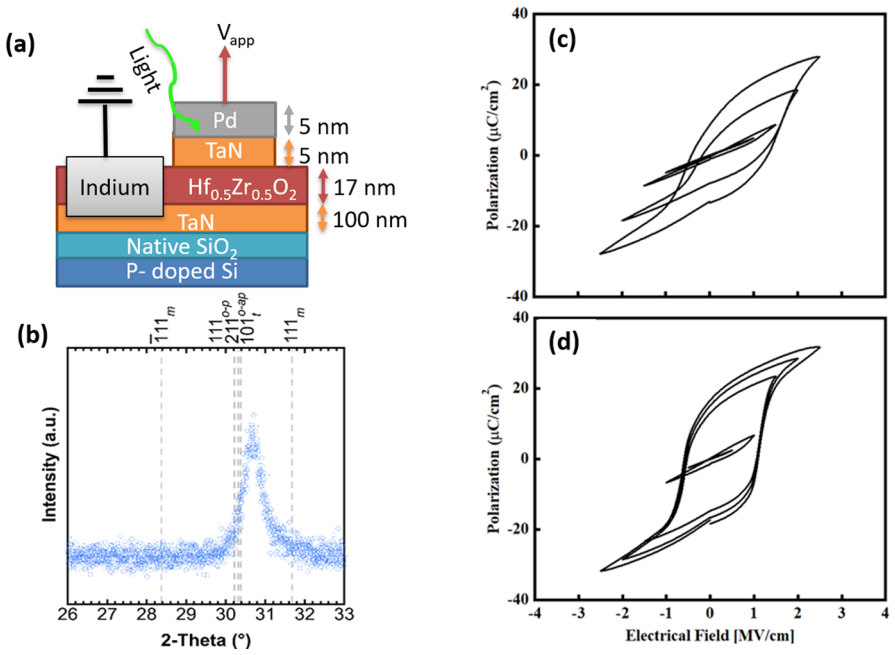

Figure 1. (a) Schematic cross section of the MFM devices used in this work illustrating the terminal bias scheme used for IPE. (b) Grazing-incidence XRD pattern of the 17 nm thick HZO films used in this study (the vertical dashed lines denote the expected positions of the monoclinic (m), polar orthorhombic (o-p), antipolar orthorhombic (o-ap), and tetragonal (t) reflections). Plots of polarization vs electric field sweeps (c) before and (d) after the wake-up process.

roles in the operation of HZO MFM devices.[21] HZO in as-fabricated devices tends to be primarily in the nonferroelectric monoclinic, tetragonal, or antipolar orthorhombic crystal structures.[21−26] Inducing ferroelectric behavior in HZO devices (waking) often requires repeated electric field cycling.[22−28] It is thought that the field cycling during waking induces the transformation of nonferroelectric tetragonal and/or antipolar orthorhombic phases to the ferroelectric orthorhombic phase and possibly the formation or redistribution of charged defects (most likely oxygen vacancies, which will be generically termed V_O^+ unless specific charge states are discussed).[6,23,25] Subsequent "poling" of the devices via application of a single 100× longer positive or negative unipolar pulse aligns the ferroelectric domains and sets the polarization state to either P↓ (positive bias on top electrode) or P↑ (negative bias on top electrode). It is also thought that the relatively long duration stress during the poling process involves the creation of V_O^+ and/or drift of V_O^+ to one of the electrode interfaces.[29,30] Due to the potential involvement of charged defects and the creation and flipping of ferroelectric (FE) domain dipoles, both the waking and poling processes might be expected to impact the energy barriers at the HZO/electrode interfaces. Although IPE measurements of the band offsets between post-deposition-annealed ferroelectric HZO and various metal electrodes were recently reported by Jenkins et al.,[21] there have been no reports on the effect of the waking and poling operations on energy barriers in these devices.

In this work, IPE was used to measure in situ HZO/electrode energy barriers in *operating* TaN/HZO/TaN metal/ferroelectric/metal (MFM) device structures for the first time. Top and bottom electrode interfaces of as-fabricated (pristine), awoken, positive poled, and negative poled devices were measured and compared. Results are discussed in light of literature V_O^+ models.

2. EXPERIMENTAL SECTION

MFM devices were fabricated following procedures published previously.[30] In brief, a blanket TaN bottom electrode was first deposited on Si using DC magnetron sputtering in Ar from a sintered TaN target. HZO was then deposited at 260 °C via plasma-enhanced atomic layer deposition (ALD) within an Oxford FlexAL II instrument. Seventeen supercycles of 6 cycles of tetrakis(ethylmethylamido)hafnium (TEMA-Hf)/O_2-plasma and 4 cycles TEMA-Zr/O_2-plasma were performed to achieve a final thickness of 17 nm with a target composition of $Hf_{0.5}Zr_{0.5}O_2$ (differential growth rates of HfO_2 and ZrO_2 result in the 6:4 cycle ratio having a composition of nearly $Hf_{0.5}Zr_{0.5}O_2$). A 17 nm thick layer of HZO was selected for this study to facilitate IPE by isolating interface limited conduction from any direct tunneling through the HZO film. Following HZO deposition, a blanket 20 nm layer of TaN was sputtered, and the sample was annealed at 600 °C for 30 s in dynamic N_2 at 1 atm within an Allwin21 AccuThermo 610 rapid thermal annealer. The top TaN was then stripped via immersion in an SC-1 bath. Finally, 5 nm TaN/5 nm Pd was then deposited through a shadow mask to form 100, 200, and 300 μm diameter dots to serve as optically transparent top electrodes. A cross-sectional schematic of the completed MFM structure is shown in Figure 1a. The phases present in the film were assessed using grazing-incidence X-ray diffraction (XRD) with a Rigaku Smartlab instrument with Cu Kα radiation.

An electrode replacement procedure was used to maximize the ferroelectric phase fraction in the HZO films, while still allowing for IPE measurements. It is well-known that performing the crystallization anneal without a top electrode leads to large monoclinic phase fractions.[6] The very thin top electrodes required for optical transparency for the IPE measurements would challenge the ability of the top electrode to provide a sufficient membrane force to prevent formation of the monoclinic phase (see, for example, ref 32). Furthermore, a 5 nm thick Pt layer would likely dewet under a 600 °C anneal, leaving large uncertainty in the actual electrode area. As such, a TaN electrode replacement procedure was used,[31] which resulted in minimal formation of the monoclinic phase, as shown in Figure 1b. Only a single reflection is observed in the 26°−33° 2θ range, which can be attributed to the ferroelectric orthorhombic phase (denoted as o-p), antipolar orthorhombic phase (denoted as o-ap), or tetragonal

https://doi.org/10.1021/acsaelm.4c00073
ACS Appl. Electron. Mater. 2024, 6, 3249−3256

phase (denoted by the subscript t). Electrical analysis shown below confirms large fractions of the ferroelectric phase.

The typical coercive field, ξ_c, of HZO is ±1.0 MV/cm. To wake-up the ferroelectric, the 200 μm devices were cycled with 5000 square waves of ±5 V (± 2.5 MV/cm) voltage pulses at 10 kHz using a Radiant Technologies Precision LC II ferroelectric tester with the drive output connected to the top electrode. The last cycle of the waking process ended with a negative bias applied to the top electrode. The 300 μm diameter electrode devices were left pristine. Once a device was awoken, a single 10 ms unipolar pulse to the top electrode of either +4 V (positive poled, P↓) or −4 V (negative poled, P↑) was used to change the state of the device, applied using an Agilent E4980A LCR meter. Both the waking and poling operations were performed at applied fields above the ξ_c of 1 MV/cm. Poling of the HZO occurred whenever the applied voltage exceeded ±2.6 V (±1.5 MV/cm) and increases with time spent under bias.

IPE measurements were performed using a house-built system. The light beam from a 150 W Xe arc lamp was passed first through a Princeton Instruments monochromator to select a single photon energy and then through bandpass filters to remove unwanted frequencies. The beam was then focused onto the top electrode of the MFM structure. Electrical contact with the bottom TaN electrode was made by scratching through the HZO dielectric layer and soldering indium to the bottom electrode. Probes were landed on a top Pd/TaN electrode and the bottom indium electrode contact. A Keithley 617 electrometer was used to measure the current, and the voltages were swept using a Yokogawa GS200 DC voltage source. Positive (negative) applied voltages correspond to emission from the bottom (top) barrier. To avoid unintentional poling of the devices, maximum applied fields were limited to ±0.88 MV/cm (±1.5 V), below ξ_c. Devices were swept between applied voltages from +1.5 V (0.88 MV/cm) to −1.5 V (−0.88 MV/cm) or from −1.5 V to +1.5 V with voltage steps of ±0.1 V. At each applied voltage, the monochromator swept the photon energy, E_p, from 1.7 to 5.5 eV, and the average current, I, was measured at each energy. The quantum yield, Y, was calculated at each photon energy using

$$Y(E_p) = (I - I_{dark})\frac{E_p}{P_{lamp}(E_p)} \quad (1)$$

where I_{dark} is the current without light (determined by taking a 30 s average of the current in the dark at each voltage) and P_{lamp} is the power of the lamp at each photon energy. Next, $Y^{1/2}$ vs E_p was plotted at each electric field in the HZO (ξ_{HZO}, corrected for the built-in electric field due to the electrode work function difference), and the most linear section was used to extract the onset threshold of IPE, φ_{thresh}. $Y^{1/2}$ was used to account for the energy distribution of carriers in the metal electrode.[15] The built-in voltage across the HZO, V_{bi}, was found by determining the voltage at which the dark current switches from negative to positive and was taken as the voltage at which ξ_{HZO} = 0 (HZO bands are flat). ξ_{HZO} was determined by subtracting V_{bi} from each applied voltage and then dividing by oxide thickness. Finally, φ_{thresh} values were plotted vs the $\xi_{HZO}^{1/2}$ to accurately account for any field-induced barrier lowering (Schottky plot). Linear fits were used to extrapolate the ξ_{HZO} = 0 barriers, φ_{bn}. The IPE φ_{bn} estimation error is ±0.1 eV for different devices but less than ±0.03 eV for repeated measurements on the same device. Devices were measured pristine, after waking, and after subsequent poling with either positive or negative voltage. To avoid potential IPE induced flipping of FE dipoles, the maximum applied field reached for most IPE measurements was ±0.88 MV/cm. The only time this field was exceeded was for the pristine (unwoken) devices. Although some of the limited number of FE domains present in the unwoken devices may have aligned with the applied field, the extracted barriers were within experimental error for sweeping from both positive to negative and negative to positive. For the positive (negative) poled devices, IPE measurements were started at +0.88 MV/cm (−0.88 MV/cm), the same polarity as the poling voltage. Thus, the polarization state was not affected by the IPE field until potentially reaching the highest fields at the opposite polarity or the last few data points of the measurement which were not used for extrapolation. Pristine and woken devices were measured with both positive and negative sweep directions. IPE measurements were started within 10 min of the preceding electrical operation.

3. RESULTS AND DISCUSSION

Shown in Figures 1c and 1d are plots of nested polarization vs applied field for a series of ±1 to ±5 V sweeps with a measurement period of 1 ms taken on 100 μm diameter Pd/TaN/HZO/TaN/Si devices (schematically shown in Figure 1a), measured before and after wake-up field cycling, respectively. The unwoken sample exhibits hysteretic response with a degree of imprint and poor saturation at positive fields. Following the wake-up process, well-saturating hysteresis is observed with coercive fields of approximately ±1 MV/cm (±1.7 V) and remanent polarization of ~20 μC/cm^2, which is typical of HZO films prepared at this thickness with TaN electrodes.[31,32]

Figure 2 shows $Y^{1/2}$ vs E_p curves for pristine, woken, and poled devices for photoinjection from either the (a) top and (b) bottom electrodes, at V_{app} = +0.7 or −0.7 V, respectively. All yield curves showed three distinct features: (i) an initial increase in yield at around 2−2.4 eV, (ii) a change in slope (decrease or reversal) at approximately 4.1 eV, (iii) an abrupt increase in yield at 5.2 eV. The initial increase of yield indicated the onset threshold of IPE, φ_{thresh}, at the voltage applied, for photoinjection of electrons from the electrode into the conduction band of the HZO. According to Afanas'ev, there are very few reports of photoemission of holes from metals into insulating oxides and none with a barrier height

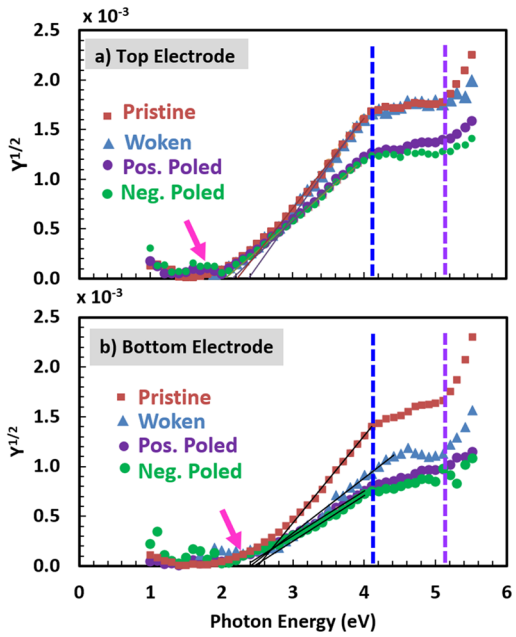

Figure 2. IPE yield plots for emission from (a) top or (b) bottom electrodes for pristine/unwoken (red squares), woken (blue triangles), positive poled (purple circles), and negative poled devices (green circles) at an applied bias of |0.7 V|. Colored lines indicate linear fits used for extrapolation of φ_{thresh}. The pink arrow indicates the approximate onset of IPE current while the purple vertical dashed line at 5.2 eV indicates the approximate onset of photoconduction. The region between the blue and purple vertical dashed lines at 4.1 and 5.2 eV, respectively, is likely due to interaction with oxygen vacancies.

https://doi.org/10.1021/acsaelm.4c00073
ACS Appl. Electron. Mater. 2024, 6, 3249−3256

more than 2 eV.[33] Holes excited by IPE would have a low lifetime and thus a low quantum yield due to the high density of filled states in the metal above the valence band of the insulator.[33,34] Wronski et al. have reported IPE of holes into semiconducting hydrogenated amorphous silicon from various metals, but all with hole barrier heights of ≤1 eV.[35]

The increase in yield at 5.2 eV was the onset of photoconduction. It corresponds to the band gap of annealed ALD HZO measured via spectroscopic ellipsometry (5.2 eV),[36] and is less than band gap values reported for either ALD HfO_2 or ZrO_2 (5.6 and 5.4 eV, respectively) measured via reflection electron energy loss spectroscopy (REELS).[14,37] The onset of photoconduction occurred at approximately 5.2 eV regardless of electric field sweep direction for both bottom and top electrodes in pristine, woken, and both negative and positive poled devices, indicating that the transformations in the crystal structure due to the waking and poling operations did not appreciably change the bandgap. The onset of photoconduction occurred at higher energy than the 4.9 eV reported by Jenkins et al. for IPE of unannealed HZO deposited by thermal ALD, which may have been impacted by band tailing, V_O^+ density, or relatively higher monoclinic phase fractions which have a lower bandgap than the orthorhombic phase.[21,38]

The change in slope seen in all curves at 4.1 eV and the yield behavior between 4.1 to 5.2 eV was consistent with an optical absorption observed between approximately 4 and 5 eV in ALD-prepared HZO that was attributed to V_O^+ as well as REELS feature starting at about 1 eV below the CB of Ar^+ sputtered HfO_2.[16−20] This energy range was also consistent with modeling and ab initio DFT calculations of V_O^+ energy levels.[30,39−41] The decreased yield slope in this range was thus likely due to photoemission from the HZO VB into oxygen vacancies competing with IPE as well as possibly neutralizing some positive charge which could inhibit IPE. The onset of the slope change remains approximately the same for pristine, woken, and poled devices for emission from both top and bottom interfaces, indicating the energy levels of these defects was not significantly impacted by these electrical operations. As discussed below, the detailed shape of the yield behavior in this region was dependent upon the interface and the operational state of the device and was likely related to the density and position of defects with respect to the interfaces.

Shown in Figure 3 are Schottky plots of φ_{thresh} vs $\xi_{OX}^{1/2}$ for emission from (a) top and (b) bottom electrodes. φ_{bn} were extracted by extrapolation to zero field and were independent of the sweep direction used to acquire yield plots (less than ±0.03 eV difference, well within experimental error). For the pristine devices, the φ_{bn} of the top TaN/HZO and bottom HZO/TaN interfaces were approximately 2.6 and 2.9 eV, respectively. Though nominally symmetric, the top and bottom interfaces experienced different processing. The bottom HZO/TaN interface was formed via ALD of HZO on TaN, whereas the top TaN/HZO interface was formed by first sputtering 20 nm of TaN on HZO and then annealing for 600 °C for 30 s in N_2. Following the annealing, this sacrificial TaN layer was stripped, and then 5 nm of new TaN was deposited. The TaN sputter deposition/annealing/stripping/redeposition sequence likely led to the greater formation of V_O^+ in the HZO near the top TaN electrode.[25,44] The V_O^+ near the surface and/or the formation of an interfacial dipole likely contributed to the lowering of the top electrode barrier in the pristine devices. Both top and bottom φ_{bn} values are within the 2.5−3.0 eV

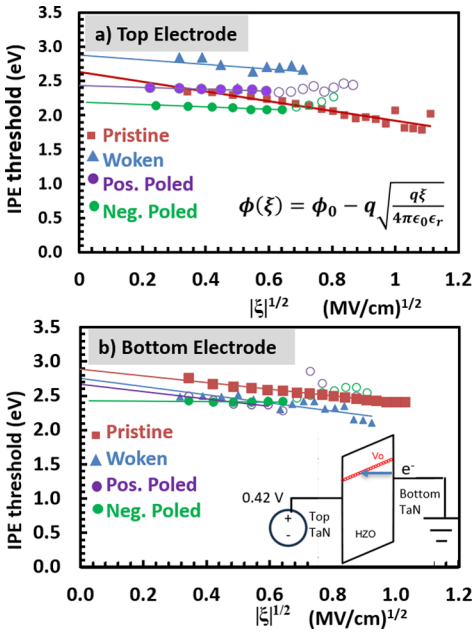

Figure 3. Schottky plots for emission from (a) top and (b) bottom electrodes for pristine, woken, and poled devices. The inset in (b) shows a band diagram with ξ_{HZO} = −0.42 MV/cm applied to top electrode, illustrating the alignment of the band of V_O^+ gap states throughout.

range reported by Jenkins et al. for bottom ALD HZO/TaN barriers with a variety of top electrode metals.[20,26] For their TaN/HZO/TaN devices, Jenkins et al. measured 2.7 eV for the top TaN/HZO barrier, within error of our result, but only 2.5 eV for the bottom HZO/TaN barrier, substantially less than the 2.9 eV seen here. The difference is likely due to differences in processing. In Jenkins et al.[21] the thermal ALD-prepared HZO was annealed directly following deposition (600 °C for 30 s in N_2), whereas in this work, HZO was deposited via plasma enhanced ALD and annealing took place after TaN deposition. The difference in φ_{bn} for nominally the same material stack emphasizes the need to measure barriers in the specific device structures used.

The waking process resulted in an increase in φ_{bn} of the top interface, from 2.6 to 2.9 eV, but no significant change in the bottom barrier. The waking procedure opens the ferroelectric hysteresis loop and involves conversion of the material from tetragonal and/or antipolar orthorhombic to polar orthorhombic (ferroelectric) and is thought to involve the redistribution/movement of oxygen vacancies (which tend to be positively charged).[22,23,29,30] As the two orthorhombic hafnia crystal phases have similar bandgaps and the tetragonal phase has a much larger bandgap,[35,38] the increase in the top electrode electron φ_{bn} is likely due to a redistribution of V_O^+ away from the top interface and toward the bulk of the material. The device thus appeared more symmetric with φ_{bn} of 2.8 and 2.9 eV for the top and bottom electrodes, respectively. Note that oxygen vacancies have been observed to move at fields around 1.5 MV/cm.[14,21,22] This is approximately equal to the coercive field but well above the maximum fields of ±0.88 MV/cm applied during IPE.

Following waking, devices were positively or negatively poled by application of a unipolar positive or negative bias pulse to the top electrode. For both P↓ and P↑, a large reduction in both top and bottom φ_{bn} was observed. For P↑

https://doi.org/10.1021/acsaelm.4c00073
ACS Appl. Electron. Mater. 2024, 6, 3249−3256

devices, the top/bottom electrode barriers were 2.2/2.4 eV, respectively, a decrease of 0.6/0.5 eV for each barrier as compared to the woken only devices. For P↓, the top/bottom electrode barriers were 2.1/2.3 eV, a decrease of 0.7/0.7 eV, respectively, as compared to the woken devices. The reduction of both barriers after both poling operations cannot be due to FE domain alignment. Poling pulses are 100× as long as the waking pulses, representing a significant stress to the FE layer, and it is likely that the generation of additional V_O^+ throughout the HZO may be responsible for barrier reduction. Movement of V_O^+ from the bulk toward the interfaces or ionization of pre-existing neutral vacancies are additional possibilities. The slightly larger decrease in the bottom barrier for P↓ as compared to the P↑ is consistent with the drift of V_O^+ toward/away from that interface during positive/negative poling, respectively, and is discussed more below. Poling polarity did not have a large impact on either the asymmetry or the top barrier. Though both barriers are slightly smaller for P↓ than for P↑, suggesting additional creation of V_O^+ throughout, the top barriers were within experimental error.

In metal-induced gap state theory, charge transfer at *intrinsic* traps at the metal/insulator interface creates an interfacial dipole that drives the Fermi level, E_F, toward the charge neutral level of the insulator, $E_{CNL,i}$, the energy at which the dominant character of the amphoteric interface states switches from donor-like in the lower part of the bandgap to acceptor-like in the upper part. A metal on an insulator will thus behave as if it has an effective work function, $\Phi_{M,eff}$, where $\Phi_{M,eff} = E_{CNL,i} + S(\Phi_{M,vac} - E_{CNL,i})$, and $S = d\varphi_{Bn}/d\Phi_{M,vac}$.[21,42] Baumgarten et al. recently proposed an approach to interpreting band alignment within the framework of this model by taking into account the impact of changes in oxygen vacancy density on $E_{CNL,i}$. They point out that $E_{CNL,i}$ should depend not only on the intrinsic (induced) interface traps but also on "extrinsic" traps such as oxygen vacancies (which are actually also intrinsic in the sense they do not involve impurities) so that $E_{CNL,i} = E_{CNL,int} - E_{CNL,def}$, where $E_{CNL,int}$ and $E_{CNL,def}$ are the charge neutral levels for the intrinsic induced interface states and the V_O^+ defects, respectively. Thus, in order to compensate for the additional positive charge introduced by additional oxygen vacancy defects, as proposed for the poled devices, the overall $E_{CNL,i}$ would need to move upward toward the CB to produce compensating negative charge in the amphoteric intrinsic interface traps below the Fermi level. This would in turn result in smaller φ_{bn}'s, consistent with what we observe.

IPE measured φ_{bn} values for pristine, woken, and poled devices are summarized in Table 1 and illustrated using energy band diagrams in Figure 4. All measured φ_{bn} were, within experimental error, independent of bias sweep direction. Φ_{bn} were found to remain stable for at least 3 months at room temperature, suggesting that V_O^+ retain their charge state and do not appreciably drift[30] when left under an internal poling field at room temperature. As seen in Table 1, the difference in measured top and bottom barriers, $\Delta\varphi_{bn}$, is consistent with electrical measurements of V_{bi}.

Table 1. IPE Measured $\varphi_{bn,top}$, $\varphi_{bn,bottom}$, $\Delta\varphi_{bn}$, and V_{bi} of TaN/HZO/TaN MFMs in Various Operational States

woken	poled	$\varphi_{bn,top}$ (eV)	$\varphi_{bn,bottom}$ (eV)	$\Delta\varphi_{bn}$ (eV)	V_{bi} (V)
unwoken	N/A	2.6	2.9	0.3	0.3
woken	no	2.8	2.9	0.1	0.1
woken	negative, P↑	2.2	2.4	0.2	0.2
woken	positive, P↓	2.1	2.3	0.2	0.1

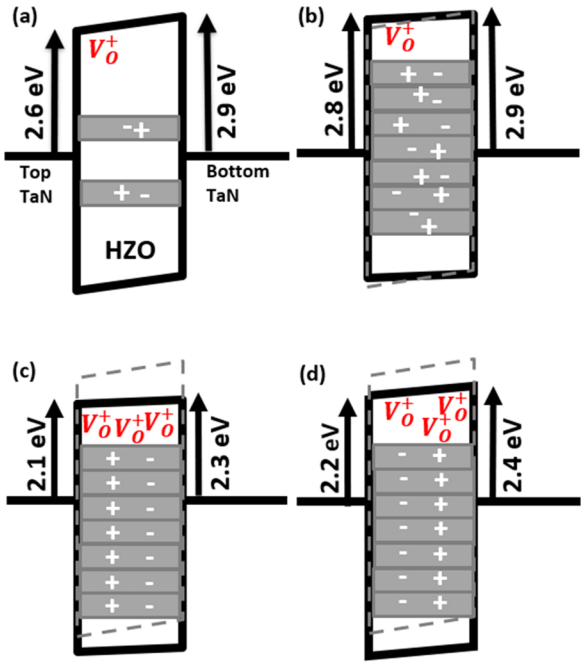

Figure 4. TaN/HZO/TaN MFM band diagrams illustrating IPE measured φ_{bn} for (a) pristine, (b) woken, (c) P↑, and (d) P↓ devices. The rectangles represent the orientation of ferroelectric domains while the red V_O^+ indicate relative position within the HZO. The dashed gray reference band diagram in (b), (c), and (d) is the pristine band diagram from (a).

The Schottky (image force) barrier lowering as ξ_{HZO} is increased may be described by

$$\varphi_{thresh}(\xi_{HZO}) = \varphi_{bn} - q\sqrt{\frac{q\xi_{HZO}}{4\pi\epsilon_0\epsilon_r}} \quad (2)$$

where q is the electronic charge, ϵ_0 is the permittivity of free space, and ϵ_r is the relative dielectric constant of the dielectric. Looking closely at Schottky plots in Figure 3a,b, it is seen that the poled devices demonstrate significantly different behavior than the pristine and woken devices. Whereas the pristine and woken/not poled devices show a negative slope throughout, as expected from eq 2, the slopes of both the positively and negatively poled devices are relatively independent of $\sqrt{\xi_{HZO}}$ at low $\sqrt{\xi_{HZO}}$ and then *positive* at $\sqrt{\xi_{HZO}}$ above ~600 $V^{1/2}$ $cm^{-1/2}$ or $\xi_{HZO} \sim 0.42$ MV cm^{-1}, still below the ξ_c. Although it is typically reported that high-k dielectrics show little to no field-induced barrier lowering in IPE measurements, a positive slope at higher ξ_{HZO} is not expected.[14,15,20] A possible explanation for the positive slope is the neutralization of V_O^+ by injected electrons at ξ_{HZO} greater than |0.42 MV cm^{-1}| (|600 $V^{1/2}$ $cm^{-1/2}$|). V_O^+ in HZO are reported/predicted to lie at around 1 eV below the conduction band edge.[32,36] As shown in the band diagram inset in Figure 4b, at |600 $V^{1/2}$ $cm^{-1/2}$| and above, the V_O^+ defect band begins to align with the Fermi level of the cathode. This energy alignment, combined with the long duration of the IPE measurement, allows the possibility of electrons tunneling into V_O^+, neutralizing them. Neutralization would effectively increase the barrier to charge transport, decreasing yield. Since the IPE characterization measurement progresses from low ξ_{HZO} to high ξ_{HZO}, φ_{bn} extrapolations

https://doi.org/10.1021/acsaelm.4c00073
ACS Appl. Electron. Mater. 2024, 6, 3249−3256

below |600 $V^{1/2}$ $cm^{-1/2}$| are not impacted by defect neutralization. As ξ_{HZO} is increased above |600 $V^{1/2}$ $cm^{-1/2}$|, however, more and more defects are accessible to tunneling from the cathode, leading to an increasing reduction in positive charge, which progressively increases φ_{thresh}. The region above |600 $V^{1/2}$ $cm^{-1/2}$| was thus excluded from the φ_{bn} extrapolations. The positive Schottky slope is only seen in the poled devices and is consistent with the strongly reduced top and bottom φ_{bn}, which would increase tunneling probability. Both the positive slope and reduced barriers are evidence in support of increased V_O^+ density or ionization of existing neutral oxygen vacancies near the interfaces and possibly throughout the poled devices.

Shown in Figure 5 are families of yield plots for emission from top (a, c, e, g) and bottom (b, d, f, h) electrodes of TaN/HZO/TaN MFM devices in the pristine (unwoken), woken, negatively poled, and positively poled states. Note that the maximum ζ_{HZO} obtained is lower for the poled devices as they typically broke down near the end of the measurement, for the negative (positive) poled devices as the oxide field was becoming increasingly positive (negative). For the positive poled devices, the IPE measurement had to be started at a lower positive field to avoid breakdown. As discussed above, the reduction in yield slope between 4 and 5.2 eV is consistent with photoemission into V_O^+. The magnitude of slope change is thus likely an indication of V_O^+ density. With the exception of the positively poled state, the slope reduction in this region is more dramatic for the top electrode than for the bottom. This suggests a higher density of V_O^+ near the top interface and indeed, in all operational states, the top barrier is smaller than the bottom barrier (see Figure 4). This is likely the result of initial processing and is consistent with defect distributions postulated by other research groups.[25,44−47] The slope change tends to be more pronounced at higher fields and peaked yield behavior (decreasing yield) can be observed in the top barrier for the unwoken, woken, and negatively poled devices, the exception being the positively poled devices. The increasingly peaked behavior at higher fields can be explained by the combination of photoemission and the alignment of Fermi level of the cathode at around 0.42 MV/cm (0.35 MV/cm is highlighted in Figure 5) with defect levels located closer and closer to the cathode (see Figure 4b), so that more and more defects are neutralized by electron tunneling.

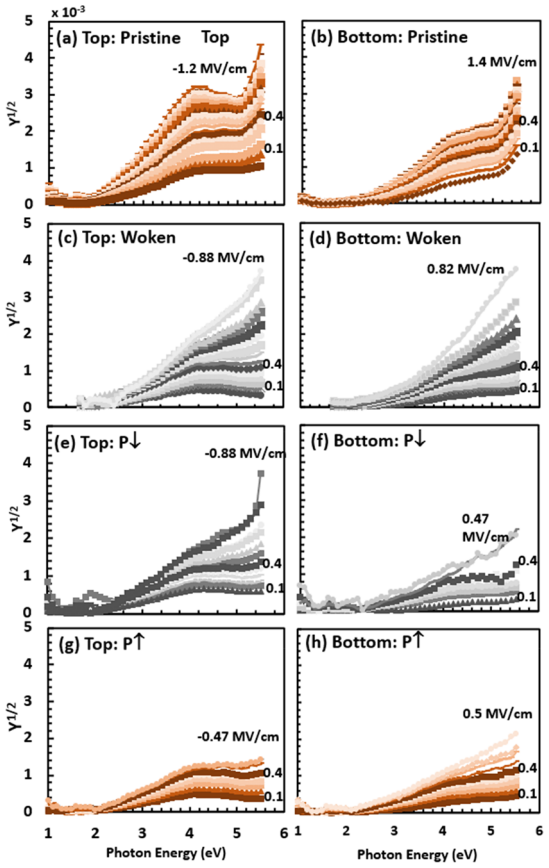

Figure 5. Plots of $Y^{1/2}$ vs incident photon energy for (a, b) pristine unwoken, (c, d) woken, (e, f) P↓, and (g, h) P↑. Highlighted in each plot are sweeps taken at ξ_{HZO} = ±0.1 MV/cm, ±0.3 MV/cm, and the maximum field attained.

For the woken state, the unchanged bottom barrier and slightly increased top barrier, suggests movement of V_O^+ away from the top interface. However, yield curves for both electrodes (Figure 5b,f) were qualitatively similar to the pristine state (Figure 5a,d), suggesting that the V_O^+ did not move very far. For the P↑, both barriers were reduced. The pronounced yield peaking (even at low voltages) for the top electrode (Figure 5c) combined with the reduced slope change in the bottom electrode as compared to woken (Figure 5g) suggests either preferential generation of V_O^+ near, or drift of V_O^+ toward, the top interface under the negative poling field. The opposite situation is observed for P↓. Here, the top electrode (Figure 5d) shows less pronounced peaking than for P↑, while the bottom electrode (Figure 5h) shows more slope change than the top electrode, consistent with movement of V_O^+ toward the bottom electrode.

In summary, the effect of the "waking" and subsequent "poling" operations on the interfacial electron barriers, φ_{bn}, of operating ferroelectric TaN/HZO/TaN MFM devices were measured for the first time. The results were found to be generally consistent with V_O^+ models, although experimental techniques such as electron paramagnetic resonance (EPR) would be required to confirm defect structure and directly measure point defect density.[48] IPE spectroscopy measurements of the top and bottom (TaN/HZO and HZO/TaN) φ_{bn} for pristine devices were 2.6 and 2.9 eV, respectively. The onset of photoconduction at 5.2 eV matched the reported bandgap of $Hf_{0.5}Zr_{0.5}O_2$. Though nominally symmetric, the top and bottom interfaces experienced different processing, likely resulting in the formation of additional V_O^+ near the top electrode, which in turn reduced the φ_{bn} of the top interface. The initial asymmetry due to processing was found to persist during device operation. The waking operation increased the top TaN/HZO barrier to 2.8 eV from 2.6 eV for the pristine (unwoken) devices while leaving the bottom HZO/TaN barrier unchanged at 2.9 eV, likely due to redistributing some V_O^+ away from the immediate vicinity of the top interface. Subsequent positive and negative poling operations were found to significantly decrease both top and bottom barriers, consistent with the formation of additional positively charged V_O^+ throughout the HZO. Poling polarity had relatively little impact. The φ_{bn} for the top interface was 2.1 eV for P↓ and 2.2 eV for P↑, while the bottom barrier φ_{bn} was 2.3 for P↓ and 2.4 eV for P↑. The slight differences between barriers in the poled devices are consistent with models of V_O^+ drift toward/away from the respective interfaces. Both interfaces of devices in all operational states showed decreased yield slope in the region

https://doi.org/10.1021/acsaelm.4c00073
ACS Appl. Electron. Mater. 2024, 6, 3249−3256

from 4 eV to the onset of photoconduction, with some devices even showing decreasing yield. This region is consistent with the absorption range of V_O^+ in HZO and the magnitude of the changes correlate with barrier heights, suggesting that this photon energy region is sensitive to V_O^+ density due to photoemission from the VB and tunnel injection from the cathode. There was no change in the onset of photoconduction regardless of poling, waking, or wait times. All barrier heights remained unchanged after several months at room temperature, indicating little change in crystal structure or migration of V_O^+, even for poled devices.

4. CONCLUSION

This work demonstrates the impact of the waking and poling operations on interfacial electron barriers in HZO MFM devices and illustrates the importance of direct in situ IPE measurements of both barriers in operating devices, measurements not generally possible with XPS. Further, this work points toward the importance of controlling oxygen vacancy concentrations and charge states as a necessary step toward developing reliable ferroelectric hafnia-based devices.

AUTHOR INFORMATION

Corresponding Author

John F. Conley, Jr. − *School of Electrical and Computer Engineering, Oregon State University, Corvallis, Oregon 97331, United States;* orcid.org/0000-0001-7407-9290; Email: John.Conley@oregonstate.edu

Authors

Jessica Haglund − *School of Electrical and Computer Engineering, Oregon State University, Corvallis, Oregon 97331, United States;* orcid.org/0000-0003-3368-7817

Takanori Mimura − *Department of Materials Science and Engineering, University of Virginia, Charlottesville, Virginia 22904, United States;* orcid.org/0000-0003-1358-2962

Jon F. Ihlefeld − *Department of Materials Science and Engineering and Charles L. Brown Department of Electrical and Computer Engineering, University of Virginia, Charlottesville, Virginia 22904, United States;* orcid.org/0000-0003-0166-8136

Complete contact information is available at: https://pubs.acs.org/10.1021/acsaelm.4c00073

Notes

The authors declare no competing financial interest.

ACKNOWLEDGMENTS

This work was performed at the Materials Synthesis and Characterization (MaSC) facility, a part of the NSF National Nanotechnology Coordinated Infrastructure (NNCI) Northwest Nanotechnology Infrastructure (NWNI) user facility at Oregon State University supported in part by the National Science Foundation (NSF) through Grant NNCI-2025489. J.H. and J.F.C. thank the Sierra Nevada Corporation for partial financial support. Thin film synthesis and polarization measurements were supported by the Center for 3D Ferroelectric Microelectronics (3DFeM), an Energy Frontier Research Center funded by the U.S. Department of Energy, Office of Science, Basic Energy Sciences, under Award DE-SC0021118.

REFERENCES

(1) Decadal Plan for Semiconductors, Full Report, 2021.

(2) Jones, N. How to Stop Data Centres from Gobbling up the World's Electricity. *Nature* **2018**, *561* (7722), 163−166.

(3) Scott, J. F.; Paz de Araujo, C. A. Ferroelectric Memories. *Science* **1989**, *246* (4936), 1400−1405.

(4) Salahuddin, S.; Datta, S. Use of Negative Capacitance to Provide Voltage Amplification for Low Power Nanoscale Devices. *Nano Lett.* **2008**, *8* (2), 405−410.

(5) Pantel, D.; Lu, H.; Goetze, S.; Werner, P.; Jik Kim, D.; Gruverman, A.; Hesse, D.; Alexe, M. Tunnel Electroresistance in Junctions with Ultrathin Ferroelectric $Pb(Zr_{0.2}Ti_{0.8})O_3$ Barriers. *Appl. Phys. Lett.* **2012**, *100* (23), 232902.

(6) Böscke, T. S.; Müller, J.; Bräuhaus, D.; Schröder, U.; Böttger, U. Ferroelectricity in Hafnium Oxide: CMOS Compatible Ferroelectric Field Effect Transistors. *In 2011 International Electron Devices Meeting* **2011**, 24.5.1−24.5.4.

(7) Mueller, S.; Summerfelt, S. R.; Muller, J.; Schroeder, U.; Mikolajick, T. Ten-Nanometer Ferroelectric Si:HfO2 Films for Next-Generation FRAM Capacitors. *IEEE Electron Device Lett.* **2012**, *33* (9), 1300−1302.

(8) Khan, A. I.; Keshavarzi, A.; Datta, S. The Future of Ferroelectric Field-Effect Transistor Technology. *Nat. Electron.* **2020**, *3* (10), 588−597.

(9) Silva, J. P. B.; Alcala, R.; Avci, U. E.; Barrett, N.; Bégon-Lours, L.; Borg, M.; Byun, S.; Chang, S.-C.; Cheong, S.-W.; Choe, D.-H.; Coignus, J.; Deshpande, V.; Dimoulas, A.; Dubourdieu, C.; Fina, I.; Funakubo, H.; Grenouillet, L.; Gruverman, A.; Heo, J.; Hoffmann, M.; Hsain, H. A.; Huang, F.-T.; Hwang, C. S.; Íñiguez, J.; Jones, J. L.; Karpov, I. V.; Kersch, A.; Kwon, T.; Lancaster, S.; Lederer, M.; Lee, Y.; Lomenzo, P. D.; Martin, L. W.; Martin, S.; Migita, S.; Mikolajick, T.; Noheda, B.; Park, M. H.; Rabe, K. M.; Salahuddin, S.; Sánchez, F.; Seidel, K.; Shimizu, T.; Shiraishi, T.; Slesazeck, S.; Toriumi, A.; Uchida, H.; Vilquin, B.; Xu, X.; Ye, K. H.; Schroeder, U. Roadmap on Ferroelectric Hafnia- and Zirconia-Based Materials and Devices. *APL Mater.* **2023**, *11* (8), 089201.

(10) Chen, Y.-F.; Hsu, L.-W.; Hu, C.-W.; Lai, G.-T.; Wu, Y.-H. Enhanced Tunneling Electro-Resistance Ratio for Ferroelectric Tunnel Junctions by Engineering Metal Work Function. *IEEE Electron Device Lett.* **2022**, *43* (2), 208−211.

(11) Waldrop, J. R.; Grant, R. W.; Kowalczyk, S. P.; Kraut, E. A. Measurement of Semiconductor Heterojunction Band Discontinuities by X-ray Photoemission Spectroscopy. *J. Vac. Sci. Technol. A* **1985**, *3* (3), 835−841.

(12) Nagata, T.; Haemori, M.; Yamashita, Y.; Yoshikawa, H.; Iwashita, Y.; Kobayashi, K.; Chikyow, T. Oxygen Migration at Pt/HfO2/Pt Interface under Bias Operation. *Appl. Phys. Lett.* **2010**, *97* (8), 082902.

(13) Jenkins, M. A.; Klarr, T.; McGlone, J. M.; Wager, J. F.; Conley, J. F., Jr. Internal Photoemission Spectroscopy Measurements of the Energy Barrier Heights between ALD SiO_2 and Ta-Based Amorphous Metals. *ECS Trans.* **2018**, *85* (13), 729−734.

(14) Jenkins, M. A.; Klarr, T.; Austin, D. Z.; Li, W.; Nguyen, N. V.; Conley, J. F., Jr. Assessment of Energy Barriers Between ZrCuAlNi Amorphous Metal and Atomic Layer Deposition Insulators Using Internal Photoemission Spectroscopy. *Phys. Status Solidi RRL - Rapid Res. Lett.* **2018**, *12* (3), 1700437.

(15) Jenkins, M. A.; McGlone, J. M.; Wager, J. F.; Conley, J. F., Jr. Internal Photoemission Spectroscopy Determination of Barrier Heights between Ta-Based Amorphous Metals and Atomic Layer Deposited Insulators. *J. Appl. Phys.* **2019**, *125* (5), 055301.

(16) Adamchuk, V. K.; Afanas'ev, V. V. Internal Photoemission Spectroscopy of Semiconductor-Insulator Interfaces. *Prog. Surf. Sci.* **1992**, *41* (2), 111−211.

(17) Afanas'ev, V. V. Electron Energy Barriers between Conducting Materials and Insulating Oxides. *In Internal photoemission spectroscopy* **2014**, 351−382.

(18) Afanas'ev, V. V.; Stesmans, A. Internal Photoemission at Interfaces of High-κ Insulators with Semiconductors and Metals. *J. Appl. Phys.* **2007**, *102* (8), 081301.
(19) Nguyen, N. V.; Kirillov, O. A.; Suehle, J. S. Band Alignment of Metal-Oxide-Semiconductor Structure by Internal Photoemission Spectroscopy and Spectroscopic Ellipsometry. *Thin Solid Films* **2011**, *519* (9), 2811−2816.
(20) Nguyen, N. V.; Kirillov, O. A.; Jiang, W.; Wang, W.; Suehle, J. S.; Ye, P. D.; Xuan, Y.; Goel, N.; Choi, K.-W.; Tsai, W.; Sayan, S. Band Offsets of Atomic-Layer-Deposited Al_2O_3 on GaAs and the Effects of Surface Treatment. *Appl. Phys. Lett.* **2008**, *93* (8), 082105.
(21) Jenkins, M. A.; Holden, K. E. K.; Smith, S. W.; Brumbach, M. T.; Henry, M. D.; Weiland, C.; Woicik, J. C.; Jaszewski, S. T.; Ihlefeld, J. F.; Conley, J. F., Jr. Determination of Hafnium Zirconium Oxide Interfacial Band Alignments Using Internal Photoemission Spectroscopy and X-Ray Photoelectron Spectroscopy. *ACS Appl. Mater. Interfaces* **2021**, *13* (12), 14634−14643.
(22) Grimley, E. D.; Schenk, T.; Sang, X.; Pešić, M.; Schroeder, U.; Mikolajick, T.; LeBeau, J. M. Structural Changes Underlying Field-Cycling Phenomena in Ferroelectric HfO2 Thin Films. *Adv. Electron. Mater.* **2016**, *2* (9), 1600173.
(23) Pešić, M.; Fengler, F. P. G.; Larcher, L.; Padovani, A.; Schenk, T.; Grimley, E. D.; Sang, X.; LeBeau, J. M.; Slesazeck, S.; Schroeder, U.; Mikolajick, T. Physical Mechanisms behind the Field-Cycling Behavior of HfO_2-Based Ferroelectric Capacitors. *Adv. Funct. Mater.* **2016**, *26* (25), 4601−4612.
(24) Fields, S. S.; Smith, S. W.; Ryan, P. J.; Jaszewski, S. T.; Brummel, I. A.; Salanova, A.; Esteves, G.; Wolfley, S. L.; Henry, M. D.; Davids, P. S.; Ihlefeld, J. F. Phase-Exchange-Driven Wake-Up and Fatigue in Ferroelectric Hafnium Zirconium Oxide Films. *ACS Appl. Mater. Interfaces* **2020**, *12* (23), 26577−26585.
(25) Cheng, Y.; Gao, Z.; Ye, K. H.; Park, H. W.; Zheng, Y.; Zheng, Y.; Gao, J.; Park, M. H.; Choi, J.-H.; Xue, K.-H.; Hwang, C. S.; Lyu, H. Reversible Transition between the Polar and Antipolar Phases and Its Implications for Wake-up and Fatigue in HfO_2-Based Ferroelectric Thin Film. *Nat. Commun.* **2022**, *13* (1), 645.
(26) Kelley, K. P.; Morozovska, A. N.; Eliseev, E. A.; Liu, Y.; Fields, S. S.; Jaszewski, S. T.; Mimura, T.; Calderon, S.; Dickey, E. C.; Ihlefeld, J. F.; Kalinin, S. V. Ferroelectricity in Hafnia Controlled via Surface Electrochemical State. *Nat. Mater.* **2023**, *22* (9), 1144−1151.
(27) Schenk, T.; Schroeder, U.; Pešić, M.; Popovici, M.; Pershin, Y. V.; Mikolajick, T. Electric Field Cycling Behavior of Ferroelectric Hafnium Oxide. *ACS Appl. Mater. Interfaces* **2014**, *6* (22), 19744−19751.
(28) McMitchell, S. R. C.; Clima, S.; Ronchi, N.; Banerjee, K.; Celano, U.; Popovici, M.; Di Piazza, L.; Van den Bosch, G.; Van Houdt, J. Elucidating Possible Crystallographic Origins of Wake-up Mechanisms in Ferroelectric Hafnia. *Appl. Phys. Lett.* **2021**, *118* (9), 092902.
(29) Starschich, S.; Menzel, S.; Böttger, U. Evidence for Oxygen Vacancies Movement during Wake-up in Ferroelectric Hafnium Oxide. *Appl. Phys. Lett.* **2016**, *108* (3), 032903.
(30) Hamouda, W.; Mehmood, F.; Mikolajick, T.; Schroeder, U.; Mentes, T. O.; Locatelli, A.; Barrett, N. Oxygen Vacancy Concentration as a Function of Cycling and Polarization State in $TiN/Hf_{0.5}Zr_{0.5}O_2/TiN$ Ferroelectric Capacitors Studied by x-Ray Photoemission Electron Microscopy. *Appl. Phys. Lett.* **2022**, *120* (20), 202902.
(31) Fields, S. S.; Jaszewski, S. T.; Lenox, M. K.; Ihlefeld, J. F. Asymmetric Electrode Work Function Customization via Top Electrode Replacement in Ferroelectric and Field-Induced Ferroelectric Hafnium Zirconium Oxide Thin Films. *Adv. Mater. Interfaces* **2023**, *10* (8), 2202232.
(32) Fields, S. S.; Cai, T.; Jaszewski, S. T.; Salanova, A.; Mimura, T.; Heinrich, H. H.; Henry, M. D.; Kelley, K. P.; Sheldon, B. W.; Ihlefeld, J. F. Origin of Ferroelectric Phase Stabilization via the Clamping Effect in Ferroelectric Hafnium Zirconium Oxide Thin Films. *Adv. Electron. Mater.* **2022**, *8* (12), 2200601.
(33) Afanas'ev, V. V. Silicon-Insulator Interface Barriers. In *Internal Photoemission Spectroscopy*, 2nd ed.; Afanas'ev, V. V., Ed.; Elsevier: Oxford, 2014; pp 255−99.
(34) Powell, R. J. Photoinjection into SiO_2: Use of Optical Interference to Determine Electron and Hole Contributions. *J. Appl. Phys.* **1969**, *40* (13), 5093−5101.
(35) Wronski, C. R.; Lee, S.; Hicks, M.; Kumar, S. Internal Photoemission of Holes and the Mobility Gap of Hydrogenated Amorphous Silicon. *Phys. Rev. Lett.* **1989**, *63* (13), 1420−23.
(36) Ihlefeld, J. F.; Luk, T. S.; Smith, S. W.; Fields, S. S.; Jaszewski, S. T.; Constantine, C.; Lu, P.; Henry, M. D.; Davids, P. S. Compositional Dependence of Linear and Non-Linear Optical Response in Crystalline Hafnium Zirconium Oxide Thin Films. *Journal of Applied Physics* **2020**, *128* (3), 034101.
(37) Alimardani, N.; King, S. W.; French, B. L.; Tan, C.; Lampert, B. P.; Conley, J. F., Jr. Investigation of the Impact of Insulator Material on the Performance of Dissimilar Electrode Metal-Insulator-Metal Diodes. *J. Appl. Phys.* **2014**, *116* (2), 024508.
(38) Jaszewski, S. T.; Calderon, S.; Shrestha, B.; Fields, S. S.; Samanta, A.; Vega, F. J.; Minyard, J. D.; Casamento, J. A.; Maria, J.-P.; Podraza, N. J.; Dickey, E. C.; Rappe, A. M.; Beechem, T. E.; Ihlefeld, J. F. Infrared Signatures for Phase Identification in Hafnium Oxide Thin Films. *ACS Nano* **2023**, *17* (23), 23944−23954.
(39) Fengler, F. P. G.; Nigon, R.; Muralt, P.; Grimley, E. D.; Sang, X.; Sessi, V.; Hentschel, R.; LeBeau, J. M.; Mikolajick, T.; Schroeder, U. Analysis of Performance Instabilities of Hafnia-Based Ferroelectrics Using Modulus Spectroscopy and Thermally Stimulated Depolarization Currents. *Adv. Electron. Mater.* **2018**, *4* (3), 1700547.
(40) Islamov, D. R.; Gritsenko, V. A.; Perevalov, T. V.; Pustovarov, V. A.; Orlov, O. M.; Chernikova, A. G.; Markeev, A. M.; Slesazeck, S.; Schroeder, U.; Mikolajick, T.; Krasnikov, G. Y. Identification of the Nature of Traps Involved in the Field Cycling of Hf0.5Zr0.5O2-Based Ferroelectric Thin Films. *Acta Mater.* **2019**, *166*, 47−55.
(41) Chai, J.; Xu, H.; Xiang, J.; Zhang, Y.; Zhou, L.; Zhao, S.; Tian, F.; Duan, J.; Han, K.; Wang, X.; Luo, J.; Wang, W.; Ye, T.; Guo, Y. First-Principles Study of Oxygen Vacancy Defects in Orthorhombic $Hf_{0.5}Zr_{0.5}O_2/SiO_2/Si$ Gate Stack. *J. Appl. Phys.* **2022**, *132* (10), 105301.
(42) Yeo, Y.-C.; King, T.-J.; Hu, C. Metal-Dielectric Band Alignment and Its Implications for Metal Gate Complementary Metal-Oxide-Semiconductor Technology. *J. Appl. Phys.* **2002**, *92* (12), 7266−7271.
(43) Baumgarten, L.; Szyjka, T.; Mittmann, T.; Gloskovskii, A.; Schlueter, C.; Mikolajick, T.; Schroeder, U.; Müller, M. Smart Design of Fermi Level Pinning in HfO_2 -Based Ferroelectric Memories. *Adv. Funct. Mater.* **2024**, *34*, 2307120.
(44) Hsain, H. A.; Lee, Y.; Lancaster, S.; Materano, M.; Alcala, R.; Xu, B.; Mikolajick, T.; Schroeder, U.; Parsons, G. N.; Jones, J. L. Role of Oxygen Source on Buried Interfaces in Atomic-Layer-Deposited Ferroelectric Hafnia-Zirconia Thin Films. *ACS Appl. Mater. Interfaces* **2022**, *14* (37), 42232−42244.
(45) Schenk, T.; Hoffmann, M.; Ocker, J.; Pešić, M.; Mikolajick, T.; Schroeder, U. Complex Internal Bias Fields in Ferroelectric Hafnium Oxide. *ACS Appl. Mater. Interfaces* **2015**, *7* (36), 20224−20233.
(46) Fengler, F. P. G.; Hoffmann, M.; Slesazeck, S.; Mikolajick, T.; Schroeder, U. On the Relationship between Field Cycling and Imprint in Ferroelectric $Hf_{0.5}Zr_{0.5}O_2$. *J. Appl. Phys.* **2018**, *123* (20), 204101.
(47) Hamouda, W.; Pancotti, A.; Lubin, C.; Tortech, L.; Richter, C.; Mikolajick, T.; Schroeder, U.; Barrett, N. Physical Chemistry of the $TiN/Hf_{0.5}Zr_{0.5}O_2$ Interface. *J. Appl. Phys.* **2020**, *127* (6), 064105.
(48) Lenahan, P. M.; Conley, J. F., Jr. Magnetic Resonance Studies of Trapping Centers in High-/Spl Kappa/ Dielectric Films on Silicon. *IEEE Trans. Device Mater. Reliab.* **2005**, *5* (1), 90−102.

https://doi.org/10.1021/acsaelm.4c00073
ACS Appl. Electron. Mater. 2024, 6, 3249−3256